Evaluation of fluctuating voltage topology with fuel cells and supercapacitors for automotive applications

Received: 4 March 2019 | Revised: 25 April 2019 | Accepted: 27 April 2019

DOI: 10.1002/er.4622

RESEARCH ARTICLE

WILEY INTERNATIONAL JOURNAL OF ENERGY RESEARCH

Evaluation of fluctuating voltage topology with fuel cells and supercapacitors for automotive applications

Qian Xun | Yujing Liu

Department of Electrical Engineering, Chalmers University of Technology, Hörsalsvägen 11, 41296 Göteborg, Sweden

Correspondence
Qian Xun, Department of Electrical Engineering, Chalmers University of Technology, Hörsalsvägen 11, 41296 Göteborg, Sweden.
Email: qian.xun@chalmers.se

Funding information
Swedish Electromobility Center project

Summary

To develop a single-stage power conversion topology in which energy storage devices can be directly coupled, a fluctuating voltage topology is applied, leading to lower cost and more compactness with the absence of DC/DC converters. This paper investigates such a topology for automotive applications where fuel cells are directly connected to the DC bus of the inverter, resulting in fluctuating voltage across the DC bus. Further, a supercapacitor pack is also introduced to maintain the power capacity and voltage stability. The hybridization principle and practical application of such a topology are then discussed in the time domain and frequency domain. Furthermore, the transient power requirement is decomposed to design the size of fuel cells and supercapacitors. Simulation results from the modeling of the fuel cell-supercapacitor powertrain demonstrate the feasibility and effectiveness of this topology. The supercapacitors can serve as a low-pass filter for the fuel cells. In conclusion, the peak power requirement can be successfully achieved because of the lowered system impedance, and the fuel cells only need to supply the average power.

KEYWORDS

fluctuating voltage topology, DC/DC converters, fuel cells, supercapacitors, low-pass filter

1 | INTRODUCTION

Transportation electrification and integration have played a key role in reducing greenhouse gas (GHG) emissions, thereby mitigating the energy crisis, and other environmental issues.[1] Automobile industries have seen significant advancement in the gradual replacement of internal combustion engine vehicles by electric vehicles (EVs). An EV is usually powered through a collector system by electricity from off-vehicle sources, or through self-contained devices to convert fuel to electricity. Today, a wide range of automotive equipment manufacturers offer a battery electric vehicle (BEV) model to the market. However, the major disadvantage of battery-powered vehicles is the time required to recharge the batteries, although a fast charging technique is being gradually developed.[2]

With a fast-refueling time, high energy density, and zero GHG emissions, fuel cells (FCs) have become an emerging focus in EV applications. Due to physical limitations of the FCs, such as low power density and slow dynamics, EVs solely powered by FCs are often criticized for their massive and bulky power unit, long start-up time, and slow power response.[3] In contrast, supercapacitors or lithium-ion batteries have the high power density and fast response to power capability. These two factors motivate the hybridization of the FCs and the addition of a secondary energy device. This hybridization is expected to take advantage of both the FCs and the secondary energy device: high-energy

density and high power density. Theoretically, power demand can always be satisfied by the hybrid energy system with downsized FCs and a well-designed power split.

The typical polarization curve of any FC shows that the output voltage is quite low and decreases with the load current.[4] Consequently, a technical challenge arises in designing an FC drive system for EVs, namely, how to deal with the variable voltage of the FC stack over the whole load range. Also, how to recover the regenerated energy during the process of braking and deceleration is still not completely developed.

The most commonly used powertrain configuration is powered by an FC stack and a small battery, with a DC/DC converter connected in between.[5] The DC/DC converter is used to keep the DC bus voltage in a relatively smooth range while the voltage of the FC varies in a controllable range.

Research on general topology is primarily concerned on how to deal with the power split between each power supply. Controlling the power distribution of such a topology is not difficult, and several control strategies have been proposed to determine the power flow between the FC and battery or supercapacitor.[6-9] However, incorporating a DC/DC converter will inevitably sacrifice some energy and power, which results in some additional losses, typically ranging from 1% to 10% depending on the load and construction of the converters,[10,11] and it would also lead to increased volume and weight of the whole system.[12]

One way of tackling these issues is to use fluctuating voltage topology where the FC is fused with a battery or a supercapacitor in a parallel fashion and directly fed to the input of the drive inverter without DC/DC converters between the power supply and the drive inverter. In this way, the power provided by each component is automatically controlled by their internal resistance, and complicated control strategies are not needed to manage the power split. The effect of the direct connection of FC and batteries,[13,14] or a combination of batteries and supercapacitors,[15] has been investigated in such a topology. However, in battery-based topologies, the power capability of the battery is often restricted because of its current limitation. A high-power rating of the FC stack is required to match the high-power demand, often in a short period. This requires full size FC stack, and large power variations during the operation may directly accelerate the aging and degradation of the FC stack.

To alleviate these drawbacks, supercapacitors are introduced to support FC in fluctuating voltage topology. Arora et al[16] analyzes the performance of different numbers of supercapacitors (one or three) directly hybridized with FC and shows that increasing the supercapacitor numbers allows for a decrease in the hydrogen amount by approximately 5%, and this also enhances the yield of FC and reduces the power contribution of FC. In Wu et al,[17] it is evident that the direct hybridized system reduces the dynamic load on the FC and also increases the hydrogen utilization efficiency. In Morin et al,[18] the power sharing between one supercapacitor and two supercapacitors, in each case coupled with FC, is analyzed. The experimental results show that the simple, direct, and passive hybridized solution could lead to higher efficiency of the system and a longer lifetime of the FC. Durability of the FC was also achieved in the fluctuating voltage topology supported by supercapacitors, as shown in Gerardin et al.[19] A detailed large-signal model of the FC-supercapacitor system was established in Turpin et al,[20] and the dynamic capabilities of the system was also analyzed.

However, within the academic literature, the analysis of fluctuating voltage topology with FC and supercapacitor for automotive applications are rare and inconclusive, and they mainly focus on the electrochemical characterization of FC and supercapacitors, with little consideration for other components in a powertrain system and the system sizing design. Therefore, this paper aims to analyze and evaluate the feasibility of fluctuating voltage topology for automotive applications by modeling each component in a vehicle system, and the sizing of FC and supercapacitor are determined by decomposition of the transient power requirement.

The remainder of this paper is organized as follows. In Section 2, the powertrain configuration and the modeling of each component, such as FC, supercapacitor, traction drive, and vehicle dynamics, are presented. In Section 3, the equivalent circuit of fluctuating voltage topology is analyzed in time domain and frequency domain, and power sharing between components is also emphasized. Simulation results are analyzed in part Section 4, and, finally, conclusions are drawn in Section 5.

2 | POWERTRAIN CONFIGURATION AND MODELING

2.1 | Powertrain configuration

Here, we consider a fluctuating voltage topology in which an FC stack and a supercapacitor pack are directly connected to the inverter to drive a vehicle system, as illustrated in Figure 1. To prevent the flow of regenerative power to the FC stack, a diode is placed between the FC and supercapacitors. In this way, both the FC and supercapacitors deal with the traction power, whereas the regenerative power is handled only by the supercapacitors.

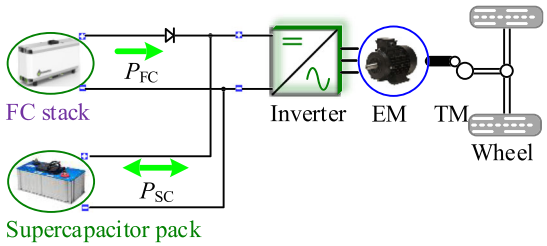

FIGURE 1 Fluctuating voltage topology [Colour figure can be viewed at wileyonlinelibrary.com]

2.2 | Drive cycle selection

To assess the functionality and performance of powertrain system under simulated real-world driving conditions, several drive cycles have been developed in different countries. In the United States, FTP-75, SC03, UDDS, US06, and LA92 are used to test for fuel consumption and pollution emissions. European countries use NEDC to measure fuel economy and other vehicular emissions, and NEDC cycle is the combination of ECE and EUDC cycles. Like Europe, Japan uses the JC08 cycle for regulatory tests.[21] The European NEDC has been replaced by the worldwide harmonized light vehicles test cycle (WLTC) for type approval testing of light-duty vehicles.[22] Because WLTC applies more realistic testing conditions, it was selected to verify the effectiveness of the fluctuating voltage topology for automotive applications in this study.

The vehicle speed and the acceleration for Class 3b with a maximum speed above 120 km/h are shown as Figure 2, and the speed is classified as low, medium, high, and extra-high according to the maximum speed level at each phase. In Figure 2, v_{max} is the maximum speed at each phase, t is the time duration, s is the distance, and a is the acceleration.

2.3 | Fuel cell model

We herein consider a generic FC model, which is available in MATLAB/Simulink and implemented with the aid of the SimPowersystems (SPS) toolbox. It is a modified version of the method described in Padulles et al[23] without consideration of the dynamic properties of the electrode regarding the reactant flow. A detailed modeling can be found in Motapon et al.[24] Figure 3 shows the schematic of the modeling. The output characteristics of the FC can be simulated by a controlled-voltage source E and a series-connected resistance r_{fc}. When considering the losses due to the reaction kinetics and species transport, the output voltage can be described as follows:

$$V_{fc} = N\left(E_{oc} - A\ln\left(\frac{i_{fc}}{i_0}\right)\cdot\frac{1}{sT_d/3+1} - r_{fc}\cdot i_{fc}\right). \quad (1)$$

The first two items in (1) represent the controlled-voltage source E, N is the number of series cells, E_{oc} is the open circuit voltage (OCV), A is the Tafel slope, i_0 is the exchange current, and T_d is the response time at 95% of the final value. Since E_{oc}, i_0, and A vary with the operation conditions, such as temperature, pressure, composition, and flow rate of hydrogen and air, these variations can be calculated by Block A, B, C as shown in Figure 3.

2.4 | Supercapacitor model

A generic supercapacitor model, available in SPS, is built according to the Stern model with the combination of Helmholtz and Gouy-Chapman models. The schematic of the modeling is shown as Figure 4.

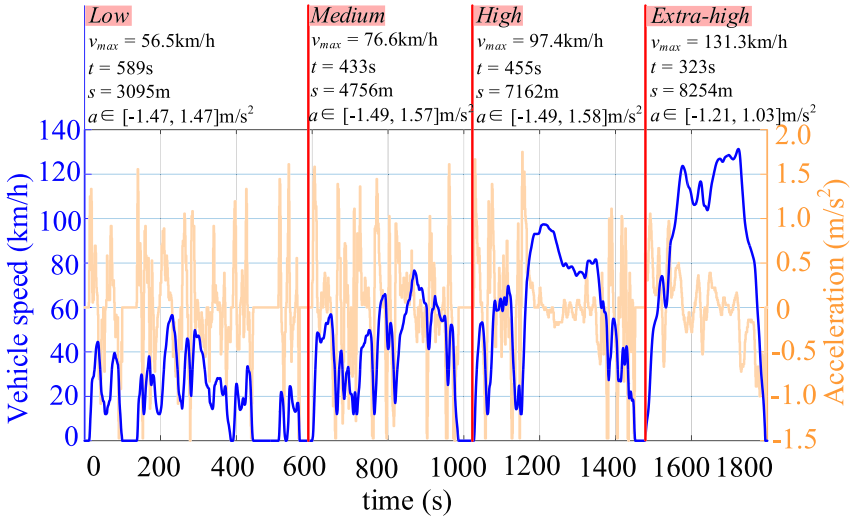

FIGURE 2 Worldwide harmonized light vehicles test cycle (WLTC) drive cycle [Colour figure can be viewed at wileyonlinelibrary.com]

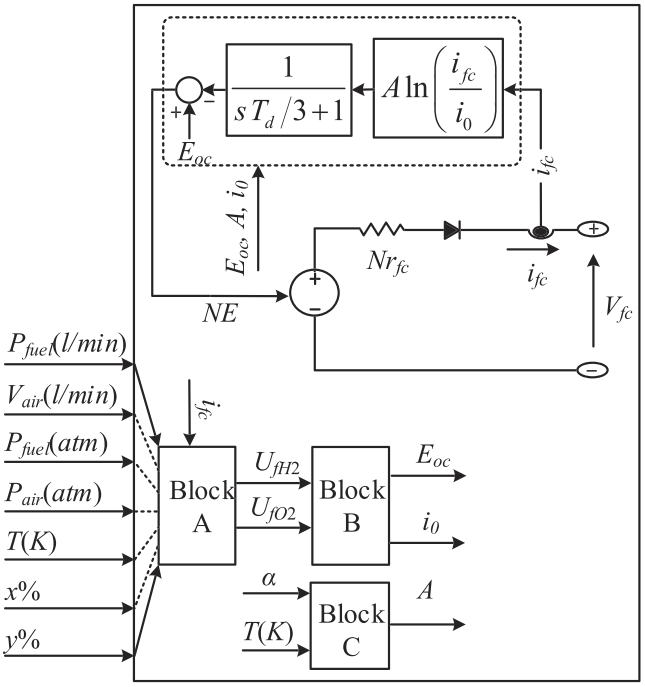

FIGURE 3 Fuel cell model

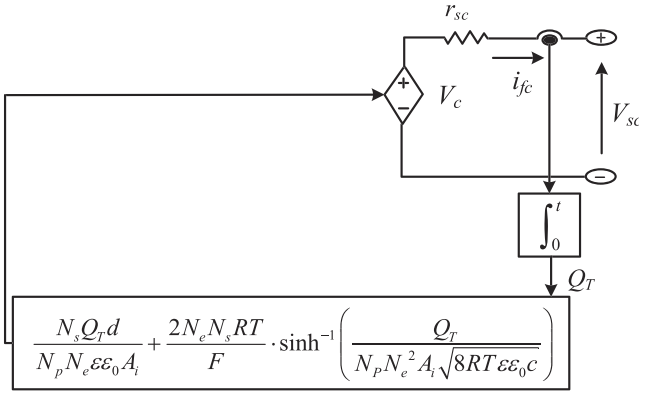

FIGURE 4 Supercapacitor model

From Figure 4, the output voltage of the supercapacitor pack may be expressed as

$$V_{SC}=\frac{N_sQ_Td}{N_pN_e\varepsilon\varepsilon_0A_i}+\frac{2N_eN_sRT}{F}\cdot\sinh^{-1}\left(\frac{Q_T}{N_PN_e^2A_i\sqrt{8RT\varepsilon\varepsilon_0c}}\right)-r_{sc}\cdot i_{sc}, \tag{2}$$

where

$$Q_T=\int i_{sc}dt. \tag{3}$$

N_s is the number of series supercapacitors, Q_T is the electric charge, d is the molecular radius, N_p is the number of parallel supercapacitors, N_e is the number of layers of electrodes, ε is the permittivity of the material, ε_0 is the permittivity of free space, A_i is the interfacial area between electrodes and electrolyte, R is the ideal gas constant, T is the operating temperature, F is the Faraday constant, and c is the molar concentration. The parameters required for the model are obtained from the datasheet in Maxwell Technologies.[25] Whereas rated values are used for the voltage, capacitance, and DC resistance, default values are used for the number of electrode layers and the molecular radius.

2.5 | Electric drive model

Electric drive system is formed by a DC/AC inverter and an electric machine in the centralized proportional system. A two-level voltage source inverter is usually used and connected with a permanent magnet synchronous motor (PMSM), shown as Figure 5.

The switches used in the study is the ideal insulated-gate bipolar transistors (IGBTs), and the traction machine is a 100-kW PMSM with peak torque of 256 Nm and rotational speed of 13 500 rpm, which is a modified and redesigned version of MCF31 machine used in Honda Clarity FC vehicle.[26]

To simulate the control characteristics of the traction drive, the flux-weakening control algorithm with maximum torque per ampere (MTPA) control has been employed to accomplish the high-speed operation. Figure 6 shows the control diagram of the drive system. The torque reference of the electric machine is decided by the pedal position of the vehicle and the torque-speed curve limited by the electric machine. The MTPA control is applied during the operation in the constant torque region, and it transfers to the flux-weakening control when it operates above the base speed. The voltage and the current are constrained by the voltage limit ellipse and current limit circle. The d-axis current and q-axis current are calculated as reference signals of the current loop and finally are used to generate drive signals of the inverter.

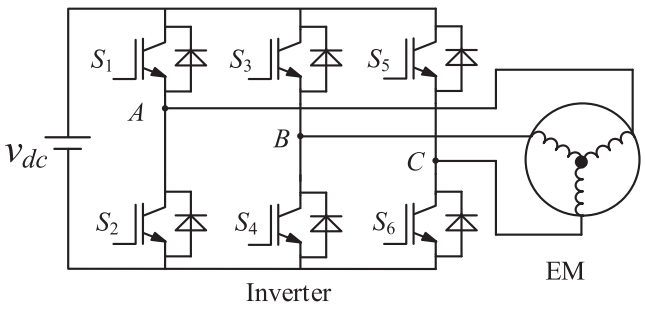

FIGURE 5 Schematic of electric drive system

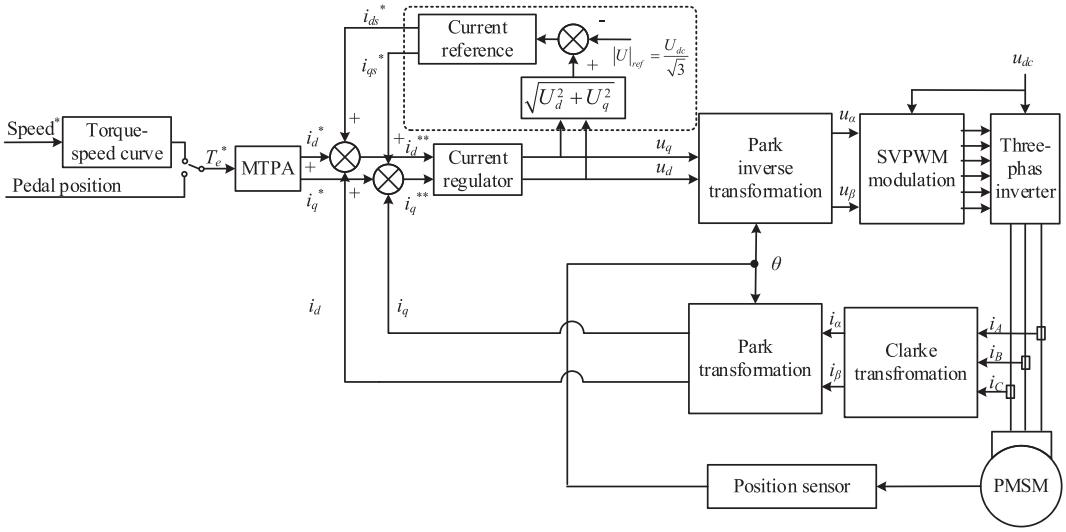

FIGURE 6 The control diagram of the permanent magnet synchronous motor (PMSM) drive system

2.6 | Mechanical drive model

The mechanical drive system incorporates transmission gear, differential, tire, and longitudinal vehicle body from the Simscape/Driveline toolbox, which is a physical model based on the Simscape environment. A signal converter block is used to interface the SPS signal and the Simscape signal. The electromechanical torque of the electric machine is transferred along the connection lines, a simple gear is employed, and the relationship of speed and torque between the electric machine and the vehicle can be written as follows:

$$n_{EM} = k_{gear}\frac{v60}{r2\pi} = k_{gear}\omega_{wheel}\frac{60}{2\pi}, \tag{4}$$

$$T_{EM} = \frac{T_{wheel}}{\eta_{gear}k_{gear}}, \tag{5}$$

where n_{EM} is the rotational speed of the electric machine, k_{gear} is the gear ratio, v is the vehicle speed, r is the wheel radius, ω_{wheel} is the wheel rotational speed, T_{EM} is the machine torque, T_{EM} is the wheel torque, and η_{gear} is the transmission efficiency, which is modeled by a total friction coefficient as a function of the rotational speed of the electric machine in rad/s.

The differential is a gear mechanism that allows the driven shaft to spin at different speed, while the tire is used to simulate the longitudinal behavior following the Magic Formula.[27] The vehicle body is used to imitate a two-axle vehicle behavior in longitudinal motion.

3 | ANALYSIS OF FLUCTUATING VOLTAGE TOPOLOGY

3.1 | Time-domain analysis

With the connection of a general load, the equivalent circuit of the fluctuating voltage topology with hybridization of FC and supercapacitor is shown in Figure 7.

Here, the FC is represented by a voltage source $v_{ocv\_fc}(t)$ and its internal resistance r_{fc}. $v_{fc}(t)$ is the terminal voltage of the FC and $i_{fc}(t)$ denotes the current of the FC. The supercapacitor is represented by Thevenin equivalent, where a nominal capacitance C and an equivalent series resistance (ESR) r_{sc} are modeled. The supercapacitor voltage $v_{ocv\_sc}(t)$ can then be regarded as a controlled voltage source and $i_{sc}(t)$ is the current flow through the supercapacitor. $v_l(t)$ and $i_l(t)$ are the voltage and the current of the load, respectively.

The terminal voltage of the FC can be simplified as

$$v_{fc} = v_{ocv\_fc} - i_{fc}r_{fc}. \tag{6}$$

Since $v_{ocv\_fc}(t)$ is the OCV, we assume that it does not vary with time.

For the supercapacitor, the relationship between the voltage and the current follows from the first-order differential equation shown below:

$$i_{sc} = C\frac{dv_{ocv\_sc}}{dt}. \tag{7}$$

The load current is supplied by the FC and the supercapacitor, and when Kirchhoff's current law is applied, we have that

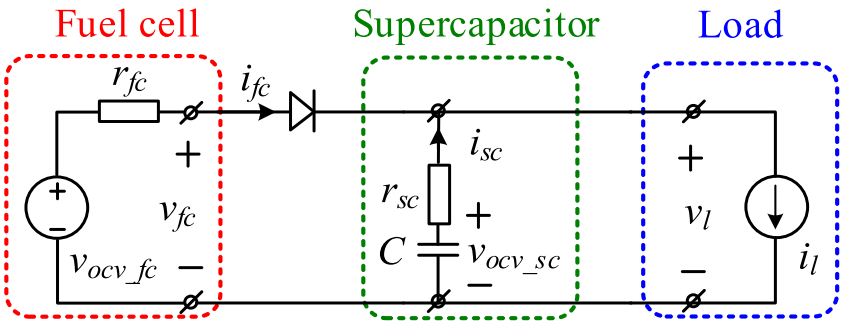

FIGURE 7 The equivalent circuit in time domain [Colour figure can be viewed at wileyonlinelibrary.com]

$$i_{sc} + i_{fc} = i_l. \tag{8}$$

If we neglect the diode losses and interconnection losses, the voltage of supercapacitor is approximately equal to that of the FC, that is, $v_{ocv\_sc} = v_{sc} = v_{fc}$. According to Kirchhoff's current law,

$$i_l - i_{fc} = C\frac{dv_{sc}}{dt}. \tag{9}$$

By putting (6) in (9), we have

$$i_l - i_{fc} = -Cr_{fc}\frac{di_{fc}}{dt}. \tag{10}$$

Since the FC voltage is approximately equal to that of the supercapacitor if we neglect losses, then the change rate of the supercapacitor voltage is the same as that of the FC. Thus, the change in FC voltage would result in a proportional change in FC current as shown in the following formula:

$$\frac{dv_{sc}}{dt} = \frac{dv_{fc}}{dt} \propto -\frac{di_{fc}}{dt}. \tag{11}$$

The dynamic behavior of the FC-supercapacitor system is schematically presented in Figure 8. When the load current varies, the currents supplied by the FC and the supercapacitor depend on the impedance of each component. Thus, power divisions between the coupling devices are balanced automatically. This is an inherent feature of this topology since the impedances of the coupling devices are different as well as the change rates of the thermodynamic potentials.

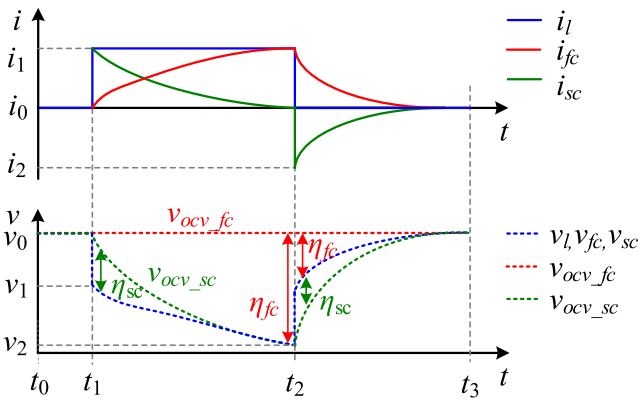

FIGURE 8 Dynamic behavior of the system [Colour figure can be viewed at wileyonlinelibrary.com]

In time range $[t_0, t_1]$, the thermodynamic OCVs of both the FC and supercapacitor are equal (v_0); namely, the two devices have the same potential in the steady state. At $t = t_1$, the load current varies from i_0 to i_1 and system voltage drops because of the load change; the OCV of the supercapacitor (v_{ocv_sc}) changes gradually, while the OCV of the FC (v_{ocv_fc}) remains constant. The difference between the load voltage and the OCV of each device represents each efficiency of the device. During $[t_1, t_2]$, a constant current i_1 is maintained; the supercapacitor gives a more significant proportion of the current at the beginning because of its lower impedance. The supercapacitor terminal voltage v_{sc} falls along with a reduced state of charge (SOC), and it gradually decreases until the load voltage becomes the same as v_{ocv_sc} again. Then, all the current is handled by the FC, since v_{ocv_fc} is constant rather than a function of current. At $t = t_2$, the load is removed; the system voltage thus increases. In $[t_2, t_3]$, the FC will charge the supercapacitor until the OCV of each component is equal again. When a negative load current is implemented, it is evident that the diode is blocked, so the FC is not in use and the supercapacitor is charged. It can be seen that FC and supercapacitors compose a current divider in time domain with the varied resistances.

3.2 | Frequency-domain analysis

The equivalent circuit in frequency domain is as shown in Figure 9.

Since the circuit is a current divider, the current flowing from the FC can be written as follows:

$$I_{FC}(j\omega) = I_L(j\omega)\cdot G(j\omega), \tag{12}$$

where $I_{FC}(j\omega)$ and $I_L(j\omega)$ are the Fourier transforms of

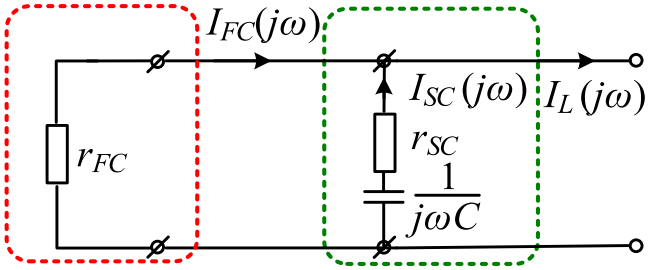

FIGURE 9 The equivalent circuit in frequency domain [Colour figure can be viewed at wileyonlinelibrary.com]

the FC current and the load current, respectively, and the transfer function from the load current to the FC current is as follows:

$$G(j\omega) = \frac{1 + j\omega C r_{SC}}{1 + j\omega C(r_{FC} + r_{SC})} = |G(j\omega)|e^{j\varphi(\omega)}, \quad (13)$$

where

$$\begin{cases} G(\omega) = \sqrt{\dfrac{1 + (\omega C r_{SC})^2}{1 + (\omega C(r_{FC} + r_{SC}))^2}} \\ \varphi(\omega) = \arctan\omega C r_{SC} - \arctan\omega C(r_{FC} + r_{SC}) \end{cases}. \quad (14)$$

Since the supercapacitor ESR is quite small compared with the FC internal resistance, one can get $r_{SC} < < r_{FC}$, and $G(j\omega)$ is a low-pass filter with a DC gain approximating 1, when $j\omega$ towards to infinity, $|G(\infty)| = \frac{r_{SC}}{r_{SC} + r_{FC}} \approx 0$. Hence, the FC supplies the DC component while the supercapacitor supplies virtually all the high-frequency current components. In the mid-frequency region, the impedance of the FC and the supercapacitor are at the same scale, and the current distribution is approximately equal. The mid-frequency characteristic depends on the pole of $\frac{1}{C(r_{FC} + r_{SC})}$. Since C and r_{SC} are coupled together, these values can be only selected from limited commercially available supercapacitor cells.

To illustrate the frequency characteristics of the FC-supercapacitor system, the normalized voltage and current of the FC are clearly observed in the fluctuating voltage topology in which the hybridized FC and supercapacitor are compared with the case with only the FC, as shown in Figure 10. The load current fluctuates between 0 and 50 A with the frequency ranging from 0.2 μHz to 2 kHz.[18]

It can be seen from Figure 10 that four operation regions can be distinguished of the voltage and current variations in fluctuating voltage topology. At low frequency region as shown in region , FC provides the major

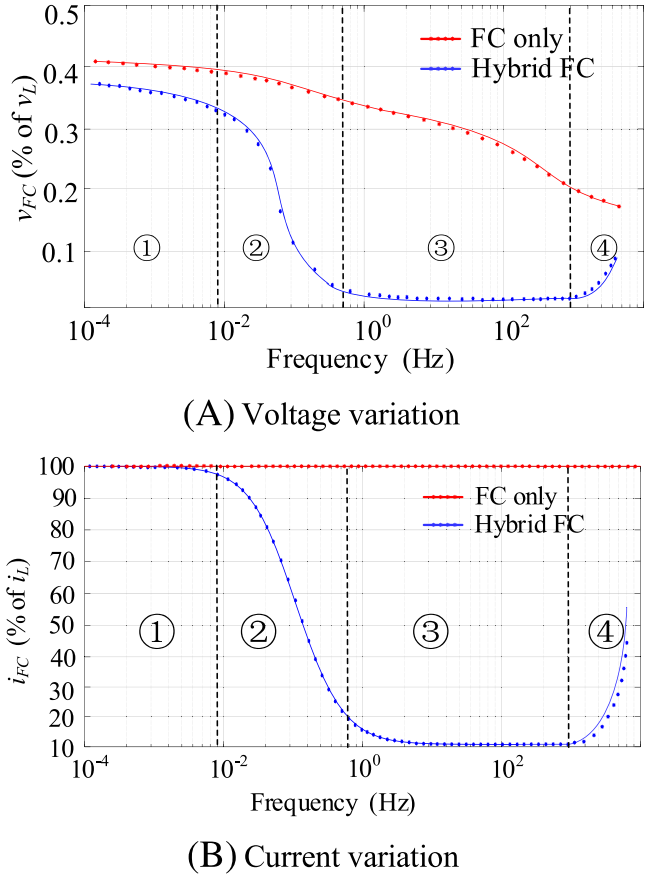

FIGURE 10 Voltage and current variations [Colour figure can be viewed at wileyonlinelibrary.com]

load current. As the frequency increases, in , the potentialities of the supercapacitor are very well exploited because of the large energy variation. In , FC supplies almost constant power because of the constant current amplitude and minimum voltage variation, and it seems to be the optimal frequency range for FC. In , the double layer capacitor of the FC provides or receives high current from the load, showing a quick variation in the SOC. The region shows a capacitive behavior of FC at high frequency.

3.3 | Transient power decomposition

For automotive applications, a vehicle is considered as a rigid body with only one axis affected by the forces that intervene in the system. Figure 11 shows the forces acting on a vehicle moving up a grade.[28]

According to Newton's second law of motion, the wheel force can be written as follows:

$$F_{wheel} = \frac{1}{2}\rho_a C_d A_f v^2 + C_r mg\cos\alpha + m\frac{dv}{dt} + mg\sin\alpha. \quad (15)$$

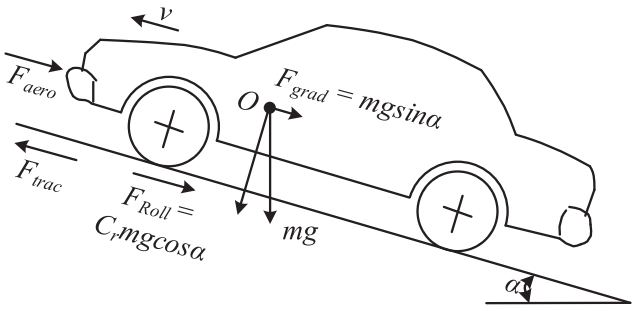

FIGURE 11 Forces acting on a vehicle

Then, the power demand during motion, including the transmission losses, can be obtained using the following:

$$P_d = F_{wheel} \cdot v + \mu \left(k_{gear} \frac{v}{r} \right)^2. \tag{16}$$

The electric machine supplies the wheel power, according to the wheel's rotational speed and the vehicle speed, the power demand of the hybrid power system can be derived from the vehicle speed.

Since the supercapacitors support FC as a low-pass filter, the cutoff frequency can be decided by the fast Fourier transform (FFT) analysis of the transient power requirement. The desired power profile for the FC is a filtered signal of the power requirement with the cutoff frequency. Then, the supercapacitor should supply the remaining power.

The sizing of the FC stack is determined by the cell polarization curve and the number of cells, and the maximum current in the polarization curve of the stack can be calculated as follows:

$$I_{\max FC} = \frac{\max(P_{FC})}{V_{FC\_\min}}, \tag{17}$$

where P_{FC} is the transient power of the FC stack and V_{FC_min} is the minimum operating voltage.

The active area of each cell is determined by the maximum current of the stack and the maximum current density of each cell, described as follows:

$$A_{fc} = \frac{I_{FC\_\max}}{J_{\max}}, \tag{18}$$

where A_{fc} is the active area and $J_{\max}$ is the maximum current density. The number of cells required to connect in series is calculated as follows:

$$N_{FC} = \frac{V_{FC\_\min}}{V_{1fc\_\min}}, \tag{19}$$

where N_{FC} is the number of cells and $V_{1fc\_\min}$ is the minimum voltage of each cell.

The sizing of the supercapacitor pack is determined by its total energy consumed during the drive cycle with the integration of the consumed power. The energy varies from $\Delta E_{\min}$ to $\Delta E_{\max}$ following the equations:

$$E_{\max} = \frac{1}{2} C V_0^2 + \Delta E_{\max} = \frac{1}{2} C V_{SC\_\max}^2, \tag{20}$$

$$E_{\min} = \frac{1}{2} C V_0^2 + \Delta E_{\min} = \frac{1}{2} C V_{SC\_\min}^2, \tag{21}$$

where C is the total capacitance of the supercapacitor pack, V_0 is the initial voltage, and $\Delta E_{\max}$ and $\Delta E_{\min}$ are the maximum and minimum energy variation compared with the initial stored energy, respectively. $V_{SC\_\max}$ and $V_{SC\_\min}$ represent the maximum and minimum operating voltage of supercapacitor pack in the system, respectively.

Since the FC stack and the supercapacitor pack share the same operating voltage, their voltage range cannot be determined arbitrarily. Figure 12 shows how the FC stack voltage and the supercapacitor pack voltage are selected.

From (20) and (21), the total capacitance and the initial voltage of the supercapacitor pack can be written as follows:

$$C = 2 \frac{\Delta E_{\max} - \Delta E_{\min}}{V_{SC\_\min}^2 + V_{SC\_\max}^2}, \tag{22}$$

$$V_0 = \sqrt{\frac{-\Delta E_{\min}}{\Delta E_{\max} - \Delta E_{\min}} \left(V_{SC\_\max}^2 + V_{SC\_\min}^2 \right)}. \tag{23}$$

The number of supercapacitor pack connected in series is determined by the maximum polarization voltage of a single FC and the maximum voltage of a single supercapacitor cell. The parallel number is determined

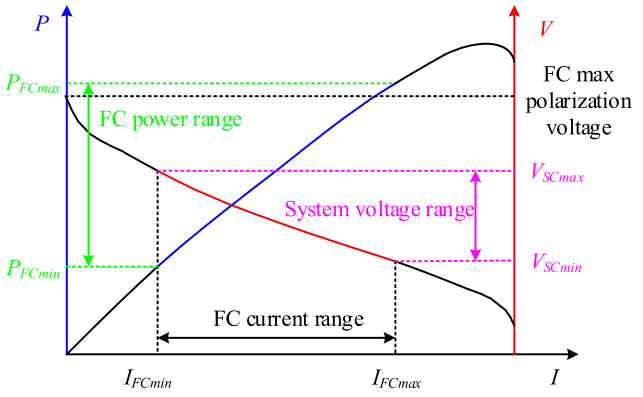

FIGURE 12 System voltage matching [Colour figure can be viewed at wileyonlinelibrary.com]

TABLE 1 Vehicle specifications

Constant (Unit)	Values
Vehicle	
Air density, ρ_a (kg/m^3)	1.18
Drag coefficient, C_d	0.26
Cross-sectional area, A_f (m^2)	2.711
Wind speed, v_{wind} (m/s)	0
Vehicle mass, m (kg)	1625
Slope, γ (%)	0
Wheel radius, r (m)	0.25
Rolling resistance coefficient, C_r	0.0098
Transmissions	
Gear ratio [−]	7.2
Total friction μ [Nm/(rad/s)]	0.01
Electric machine	
Stator phase resistance R_s (ohm)	0.0083
D-axis inductance L_d (H)	1.74e^{-4}
Q-axis inductance L_q (H)	2.92e^{-4}
Flux linkage (vs)	0.071
Pole pairs	4
Initial conditions [ω_m θ_m i_a i_b]	[0 0 0 0]
Fuel cell	
Voltage @ 0A and 1A	[336, 328]
Nominal operating point [I_{nom} (A), V_{nom} (V)]	[160, 256]
Maximum operating point [I_{end} (A), V_{end} (V)]	[200, 400]
Number of cells	368
Nominal stack efficiency (%)	55
Operating temperature (°C)	95
Nominal air flow rate (lpm)	1698
Nominal supply pressure [fuel (bar), air (bar)]	[3 3]
Nominal composition (%) [H_2, O_2, H_2O]	[9.95, 21, 1]
Fuel cell response time (s)	2
Supercapacitor	
Rated capacitance (F)	28.8
Equivalent DC series resistance (ohms)	33.04e-3
Rated voltage (V)	336
Number of series capacitors	118
Number of parallel capacitors	1
Initial voltage (V)	325
Operating temperature (°C)	25
Number of layers*	1
Molecular radius (m)*	1e-9
Permittivity of electrolyte material (F/m)	6.02e-10

*Represents the estimated value.

by the total capacitance of the pack and the single cell capacitance.

$$\begin{cases} N_{SC\_s} = \dfrac{N_{FC} V_{1fc\max}}{V_{1sc\max}} \\ N_{SC\_p} = \dfrac{C N_{SC\_s}}{C_{1sc}} \end{cases}, \tag{24}$$

where N_{SC_s} is the series number and $V_{1fc\max}$ and $V_{1sc\max}$ are the maximal voltage of a single FC and supercapacitor cell, respectively. N_{SC_s} is the parallel number, and C_{1sc} is the capacitance of a single supercapacitor cell.

4 | SIMULATION RESULTS AND SYSTEM EVALUATION

4.1 | Vehicle specifications

Table 1 shows the vehicle specifications used in this study and the input parameters for the model of electric machine, FC, and supercapacitor.

Figure 13 shows all the forces during the drive cycle except the grading force, since the angle of road inclination is 0 in the simulation. The most dominating force is due to the acceleration even though the time duration is rather short. In contrast, the rolling friction force is more significant than the air drag force at the lower speed range, up to 80 km/h where they are comparable.

The performance of the drive system is evaluated. The torque, speed, current, and voltage of the PMSM are shown in Figure 14.

The measured torque can follow the reference torque all the time, and we can get the gear ratio is about 7.2 from the rotor speed and the vehicle speed. This matches the simulation data shown as Table 1. When the electric machine operates below the base speed, the MTPA is applied, and for PMSM, it is equivalent to the control algorithm of $i_d = 0$. When the machine operates above the base speed, the flux weakening control is used, and we see the d-axis current and voltage are negative.

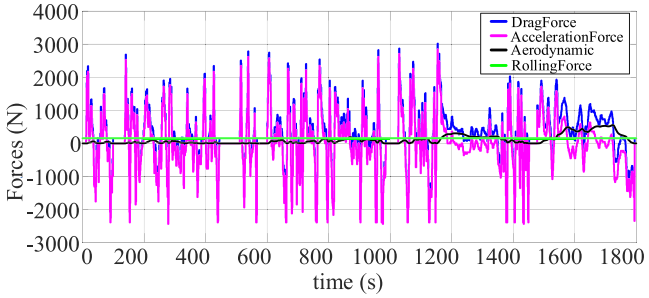

FIGURE 13 Forces analysis [Colour figure can be viewed at wileyonlinelibrary.com]

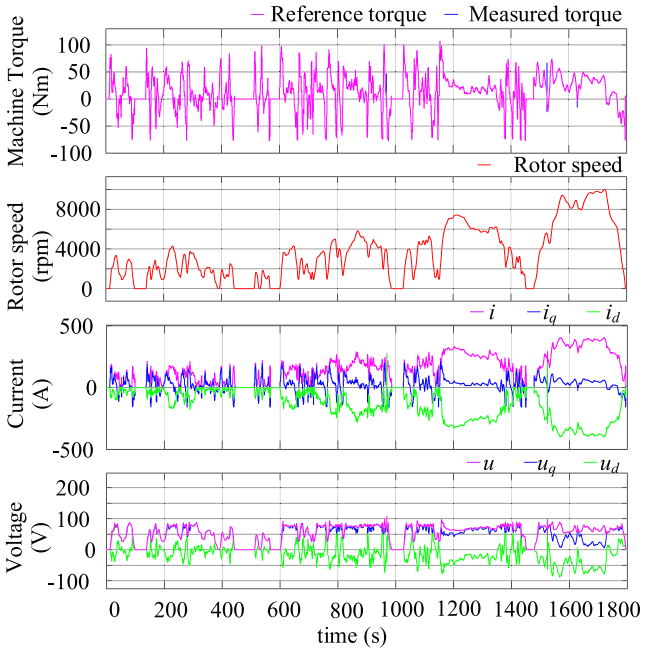

FIGURE 14 Torque, speed, current and voltage of permanent magnet synchronous motor (PMSM) [Colour figure can be viewed at wileyonlinelibrary.com]

4.2 | Power distribution

The power demand to overcome each force, including friction, is as shown in Figure 15. The power variation is similar to the force variation. The acceleration power dominates at lower speed phase because of the frequent acceleration. The powertrain losses increase with the speed, and the air drag power due to the aerodynamic also increases with the cubic of speed; thus, the total power demand is higher at extra-high-speed phase even though the acceleration is relatively lower.

In the simulation, we assume that the total drag power demand is the power requirement for the FC and supercapacitors. To visualize the energy for the drive cycle further, the power distribution is plotted as power versus time and shown in Figure 16. P_{EM} is the power

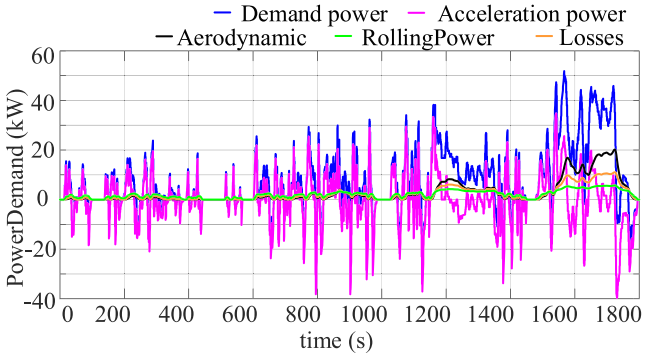

FIGURE 15 Power demand [Colour figure can be viewed at wileyonlinelibrary.com]

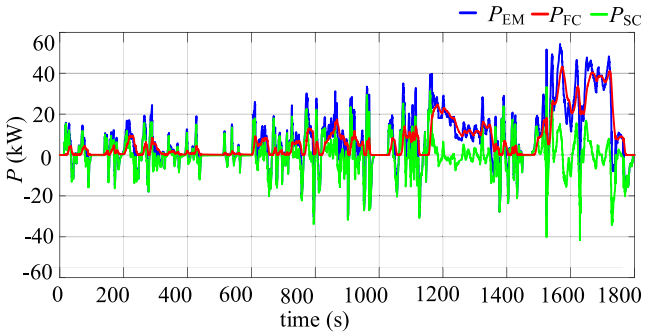

FIGURE 16 Power distribution [Colour figure can be viewed at wileyonlinelibrary.com]

requirement for EV during the test, and P_{FC} is the power provided by the FC, and P_{SC} is the power supplied by the supercapacitors. P_{FC} is relatively flat despite the dramatic variation of P_{EM}. The large transient power covered by the supercapacitor (P_{SC}) enables the FC to get rid of the large transient power rate when the vehicle accelerates or decelerates because of the smaller internal impedance of the supercapacitor. This gives the benefit of reducing the degradation of the FC and extending its lifetime.

The power samples of the FC from the simulation are sorted in descending order; in this way, the area below the curve corresponds to the energy. The outcomes, for the power of each devices, are given in Figure 17. The power demand for the traction machine and the power coming from the supercapacitor are also included. Note that the same sorting has been used for all the power signals in Figure 17; thus, all are sorted in descending order of the FC power. The FC supplies the positive power all the time, and the power edge of electric machine in positive area is almost similar to that of the supercapacitor in same time range, the only difference being that the FC provides more when at higher power demand. The power provided by FC has a similar varying trend with the electric machine demand power, which is that the power of FC decreases with the decrease of the power demand of electric machine. Meanwhile, the supercapacitor takes care of the quick variation in power demand, and in the regenerative mode, the area of supercapacitor is bigger than that of power demand, since the supercapacitors absorb the energy from the FC and the load. Also, the regenerative energy of supercapacitor is 1.38 kWh, which is almost the same as its propulsion energy, because the supercapacitor removes the peak power from the load.

4.3 | Output characteristics

Figure 18 shows the voltage, current of the FC, and supercapacitor and the SOC of the supercapacitor.

Because of the direct fusion of energy storage devices into the inverter's DC bus, the FC and supercapacitor share the same voltage, and the smaller internal impedance makes the supercapacitor supply more current at the transient state. This gives the characteristics of downsized rated power of the FC. Since there is no limitation to charging and discharging current, the

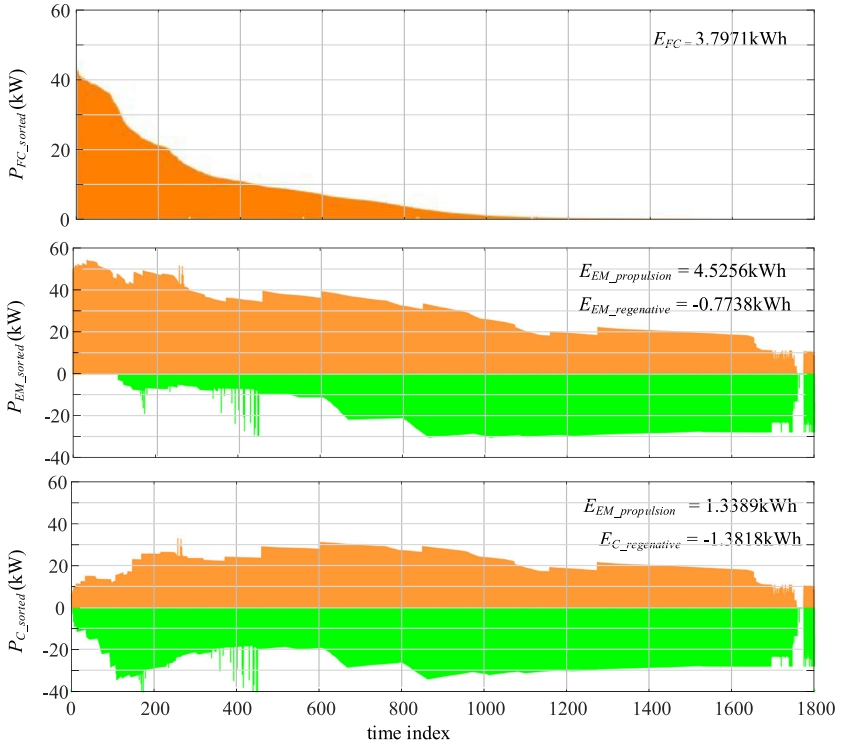

FIGURE 17 Sorted power distribution [Colour figure can be viewed at wileyonlinelibrary.com]

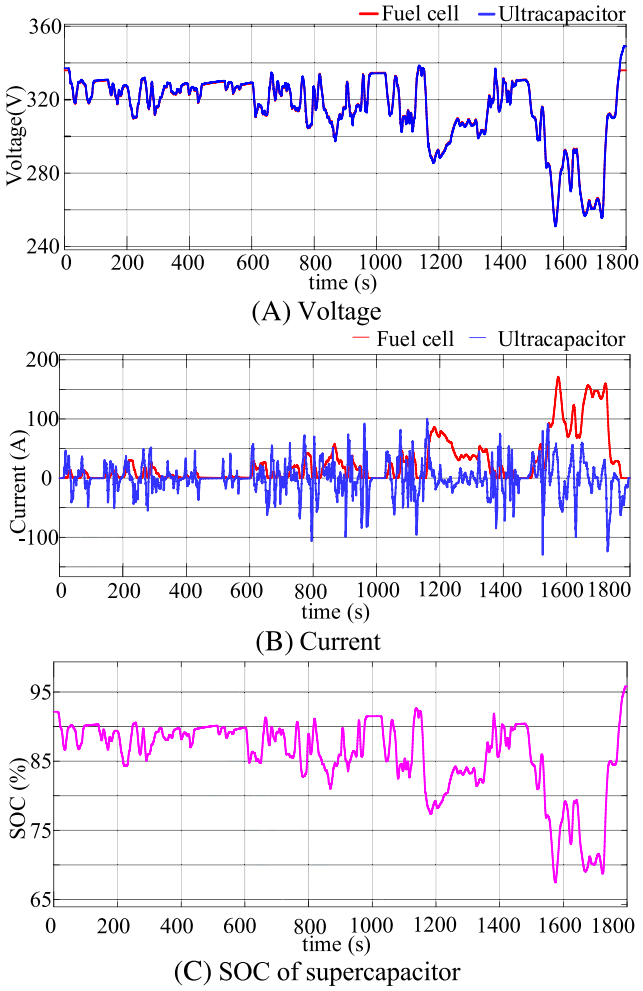

FIGURE 18 Output characteristics of FC and supercapacitor [Colour figure can be viewed at wileyonlinelibrary.com]

supercapacitor can absorb or supply more regenerative power compared with battery. In Figure 18C, the SOC of the supercapacitor gives no distinct change at the end of the test when compared with the beginning of the drive cycle, since the supercapacitor removes the power peaks from the load cycle.

To verify the feasibility of the varied DC link voltage in a vehicle system, Grunditz and Thiringer[29] has analyzed the efficiency of the electric machine as slightly decreased at lower voltage. Hence, the efficiency is somewhat increased as the base speed and high-efficiency area increase with the higher voltage. The efficiency of the inverter is mostly higher at lower voltage levels in the same torque and speed operating point, due to lower switching losses. Regarding to the acceleration characteristics from 0 to 100 km/h of the BEV under different initial SOC condition, the acceleration time is slightly shorter at higher initial SOC, which means higher voltage can lead to better acceleration characteristics. For the acceleration characteristics, Xun et al[30] shows that the vehicle with FC-supercapacitor passive connection can speed up to 100 km/h in 9 seconds, and there is no difference when compared with the conventional FC-battery powertrain configuration with the connection of a DC/DC converter.

5 | CONCLUSIONS

In this paper, the feasibility of a fluctuating voltage topology, in which FCs and supercapacitors are directly connected, for automotive applications has been analyzed and evaluated. This topology has the advantage of low cost and compactness due to the absence of DC/DC converters. Simulation results show that the fluctuating voltage topology makes it possible to reduce the power demand of the FC, and the dynamic loading drawn from the FC is also decreased when the rapid load cycling is applied. Due to the smaller impedance, the supercapacitors assist the FC as a low-pass filter to remove the peak from the load, and the FC only supplies the average power to the load. These improvements give the FC a longer lifetime.

Due to the uncontrollable power sharing between FCs and supercapacitors in the fluctuating voltage topology, the sizing and parameters of each component cannot be arbitrarily selected from available commercially products. The high energy density and high power density of FC and supercapacitors can be made full use only when the parameters of FC, supercapacitors, and electric machine as well as its controller are carefully designed. The DC link voltage always varies in fluctuating voltage topology, and further research is needed to investigate the characteristics, efficiency, and performance of such a vehicle system.

ACKNOWLEDGEMENT

This work was supported by the Swedish Electromobility centre and the Swedish Energy Agency.

ORCID

Qian Xun https://orcid.org/0000-0001-5344-5298

REFERENCES

1. Ahmad A, Alam MS, Chabaan R. A comprehensive review of wireless charging technologies for electric vehicles. *IEEE Trans Transport Electrification*. 2018;4(1):38-63.

2. Habib S, Khan MM, Abbas F, Sang L, Shahid MU, Tang H. A comprehensive study of implemented international standards, technical challenges, impacts and prospects for electric vehicles. *IEEE Access*. 2018;6(3):13866-13890.

3. Alrewq M, Albarbar A. Investigation into the characteristics of proton exchange membrane fuel cell-based power system. *IET Sci Meas Technol*. 2016;10(3):200-206.
4. Jang M, Ciobotaru M, Agelides VG. Design and implementation of digital control in fuel cell system. *IEEE Trans Ind Inf*. 2013;9(2):1158-1166.
5. Souleman Njoya M., Tremblay O, Member IEEE, Dessaint L-A. A generic fuel cell model for the simulation of fuel cell vehicles. IEEE Conference on Vehicle Power and Propulsion Conference, 2009, Sept. pp. 172–1729.
6. Zeng X, Wang J. Optimizing the energy management strategy for plug-in hybrid electric vehicles with multiple frequent routes. *IEEE Trans Control Syst Technol*. 2017;27(1):1-7.
7. Gujarathi PK, Shah V, Lokhande M. Fuzzy logic-based energy management strategy for converted parallel plug-in hybrid electric vehicle. 8*th Control and System Graduate Research Colloquium*, 2017, pp. 185–190.
8. Elsayed WM, Estima JO, Boccaletti C, Marques Cardoso AJ. Energy management strategy of a propulsion system with supercapacitors for electric and hybrid vehicles. International Power Electronics and Motion Control Conference, 2016, pp. 1210–1215.
9. Eckert JJ, F. Silva LCA, Santiciolli FM, dos Santos Costa E, Corrêa FC, Dedini FG. Energy storage and control optimization for an electric vehicle. *Int J Energy Res*. 2018;42(11):3506-3523.
10. Garrigós A, Blanes JM, Carrasco JA, Lizán JL, Beneito R, Molina JA. 5 kW DC/DC converter for hydrogen generation from photovoltaic sources. *Int J Hydrogen Energy*. 2010;25: 6123-6130.
11. Kim M-J, Peng H. Power management and design optimization of fuel cell/battery hybrid vehicles. *J Power Sources*. 2007;165(2): 819-832.
12. Ortega M, Jurado F, Valverde M. Novel topology for DC/DC unidirectional converter for fuel cell. *IET Power Electron*. 2014;7(3):681-691.
13. Nishizawa A, Kallo J, Garrot O, Weiss-Ungethüm J. Fuel cell and Li-ion battery direct hybridization system for aircraft applications. *J Power Sources*. 2013;222(1):294-300.
14. Bernard J, Hofer M., Hannesen U., Toth A, Tsukada A, Büchi FN, Dietrich P. Fuel cell/battery passive hybrid powertrain with active power sharing capability. *IEEE Vehicle Power and propulsion conference*, Lille, France, 2010, 1–3 Sept., pp. 1-5.
15. Kuperman A, Aharon I, Kara A, Malki S. A frequency domain approach to analyzing passive battery-supercapacitor hybrids supply periodic pulsed current loads. *Energ Conver Manage*. 2011;52(12):3433-3438.
16. Arora D, Gérardin K, Raël S, Bonnet C, Lapicque F. Effect of supercapacitors directly hybridized with PEMFC on the component contribution and the performance of the system. *J Appl Electrochem*. 2018;48(6):691-699.
17. Wu B, Parkes MA, Yufit V, et al. Design and testing of a 9.5 kW proton exchange membrane fuel cell-supercapacitor passive hybrid system. *Int J Hydrogen Energy*. 2014;39(15):7885-7896.
18. Morin B, Van Laethem D, Turpin C, et al. Direct hybridization fuel cell-supercapacitor. *Fuel Cells*. 2014;14(3):500-507.
19. Gerardin K, Rael S, Bonnet C, Arora D, Lapicque F. Direct coupling of PEM fuel cell to supercapacitors for higher durability and better energy management. *Fuel Cells*. 2018;18(3):315-325.
20. Turpin C, Van Laethem D, Morin B, et al. Modelling and analysis of an original direct hybridization of fuel cells and ultracapacitors. *Math Comput Simul*. 2017;131:76-87.
21. Grunditz EA, Thiringer T. Performance analysis of current BEVs based on a comprehensive review of specifications. *IEEE Trans Transport Electrification*. 2016;2(3):270-289.
22. https://www.dieselnet.com/standards/cycles/wltp.php#intro.
23. Padulles J, Ault GW, McDonald JR. An integrated SOFC plant dynamic model for power systems simulation. *J Power Sources*. 2000;86(1/2):495-500.
24. Motapon SN, Tremblay O, Dessaint L-A. Development of a generic fuel cell model: application to a fuel cell vehicle simulation. *Int J Power Electron*. 2012;4(6):505-522.
25. Maxwell Technologies. K2 ultracapacitors-2.85/3400F. Datasheet. Document number: 3000619-EN.1.
26. Fukushima T, Iwai A, Yamaguchi N, Shinoki H. Electric drive motor for fuel cell vehicle FCX clarity. *Honda R&D Tech Rev*. 2009;21(1):63-70.
27. Pacejka HB. *Tire and vehicle dynamics*. Oxford: Elsevier science; 2005.
28. Ramakrishnan K, Stipetic S, Gobbi M, Mastinu G. Optimal sizing of traction motors using scalable electric machine model. *IEEE Trans Transport Electrification*. 2017;PP(99):1-1.
29. Arfa Grunditz E, Thiringer T. Characterizing BEV powertrain energy consumption, efficiency and range during official and drive cycles from Gothenburg/Sweden. *IEEE Trans Veh Technol*. 2016;65(6):3964-3980.
30. Xun Q, Liu Y, Holmberg E. A comparative study of fuel cell electric vehicles hybridization with battery or supercapacitor. *International Symposium on Power Electronics, Electrical Drives, Automation and Emotion*, Italy, 2018, pp. 390–395.

How to cite this article: Xun Q, Liu Y. Evaluation of fluctuating voltage topology with fuel cells and supercapacitors for automotive applications. *Int J Energy Res*. 2019;43:4807–4819. https://doi.org/10.1002/er.4622